VI International Conference on Computational Methods for Coupled Problems in Science and Engineering
COUPLED PROBLEMS 2015
B. Schrefler, E. Oñate and M. Papadrakakis(Eds)

COUPLED INVERSE PROBLEMS AND VISUALIZATION OF ATMOSPHERE-OCEAN SYSTEM

SERGEY I. KABANIKHIN[*,†] **AND OLGA I. KRIVOROTKO**[*,†]

[*]Institute of Computational Mathematics and Mathematical Geophysics SB RAS
(ICM&MG SB RAS)
Prospect Ak. Lavrentjeva 6, 630090, Novosibirsk, Russia
e-mail: kabanikhin@sscc.ru, web page: http://labmpg.sscc.ru/kabanikh.html

[†]Novosibirsk State University (NSU)
Pirogova street 2, 630090, Novosibirsk, Russia
e-mail: krivorotko.olya@mail.ru, web page: http://labmpg.sscc.ru/krivorotko.html

Key words: Shallow Water Equations, Dirichlet Problem, Conjugate Gradient Method, Combined Data, Visualization System.

Abstract. We investigate two different inverse problems of determining the tsunami source using two different additional data, namely underwater measurements and satellite wave-form images, and combination of these two inverse problems. We investigate gradient-type methods for inverse problem solutions and show that combination of two types of data allows one to increase stability and convergence of numerical inverse problem solutions. Results of numerical experiments of the tsunami source reconstruction are presented and discussed. We present the 3D GIS visualization and information atmosphere-ocean system with embedded described mathematical tools of simulation of processes in atmosphere and ocean.

1 INTRODUCTION

Atmosphere-Ocean system is mathematically described by systems of hyperbolic equations. The parameter identification of Atmosphere-Ocean system using combined additional measurements is called coupled inverse problem for hyperbolic equations. These problems are ill-posed, *i.e.* their solutions are not unique or/and unstable, and should be regularized [1, 2].

As an example we consider coupled inverse source problem for the linear shallow water equations that use for describing long waves (tsunamis). Most suitable physical models related to simulation of tsunamis are based on shallow water equations (1), [3, 4]. There exist many numerical approaches for solving shallow water equations such as finite-difference, finite volume, finite element, *etc* [5]. An overview of methodologies and techniques related

to estimation of tsunami source characteristics are given in [6, 7, 8, 2]. The most of them consists in determining the tsunami source using additional measurements of a passing wave (this problem is often called inverse tsunami problem) such as DART (Deep-ocean Assessment and Reporting of Tsunamis) buoys positioned on the ocean floor, tide gauges measurements, satellite wave-form images, *etc.* Our goal is to reconstruct the tsunami source using a combination of two types of data: DART buoys and satellite wave-form image. We show that using a combination of two types of data allows one to increase the stability and efficiency of tsunami source reconstruction [9, 10].

The paper is organized as follows. In Section 2 we describe the statement of three inverse problems. In Section 3 we consider a variational formulation of the inverse tsunami problem for two types of measured data: DART data (inverse problem 1) and satellite image data measured on the part of the water surface (inverse problem 2), and then we consider the combined inverse problem (inverse problem 3). We compare two inverse problems and their combination and show the benefits of usage of combined data. Results of numerical experiments of the tsunami source reconstruction are presented in Section 4. In Section 5 we present 3D GIS visualisation and information software for tsunami simulation and run-ups with real bathymetry for the specified sea coast, as well as modelling of earthquakes, floods and other natural hazards.

2 STATEMENT OF THE PROBLEMS

The ocean domain being considered is bounded from above by the free water surface $\eta(x, y, t)$, and from below, by the bottom relief $H(x, y) > 0$. We assume that the computational time T is not large enough for the wave to reach the edges of the domain, and therefore we can set homogeneous boundary conditions at the boundary of the domain $\Omega := (0, L_x) \times (0, L_y)$ (figure 1). We formulate the initial boundary-value problem in the Cartesian coordinate system

$$\begin{cases} \mathcal{L}\eta := \eta_{tt} - \operatorname{div}(gH(x,y)\operatorname{grad}\eta) = 0, & t \in (0,T); \\ \eta|_{t=0} = q(x,y), \quad \eta_t|_{t=0} = 0, & (x,y) \in \Omega; \\ \eta|_{\partial\Omega_T} = 0, & \Omega_T := \Omega \times (0,T) \end{cases} \tag{1}$$

for the linear equations of shallow water theory in terms of the free surface without external forces, *e.g.* the Coriolis force and bottom friction [4]. Here $H \in \mathbf{H}^1(\Omega)$ is a known function describing the bottom relief (bathymetry), $q \in \mathbf{H}^2(\Omega)$ is a tsunami source which is supposed to have a compact support belonging to Ω, $g = 9.8\ [m/s^2]$. Further, we will use notation $c(x, y) = \sqrt{gH(x, y)}$ that describes the tsunami propagation velocity according to the long-wave theory.

The direct tsunami problem (1) consists in determining of a function $\eta \in C(\Omega_T; \mathbf{H}^2(\Omega))$ in the domain Ω by known functions $H(x, y)$ and $q(x, y)$.

Let us consider three inverse problems for linear shallow water equations:

Inverse problem 1 (IP 1): find $q(x, y)$ from (1) using function $H(x, y)$ and data

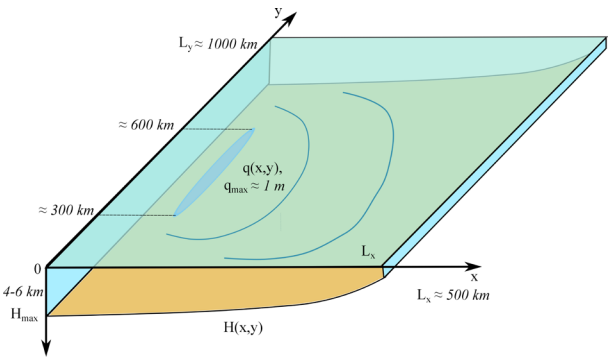

Figure 1: Domain of calculation of direct and inverse problems.

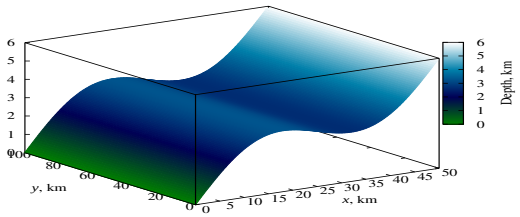

Figure 2: The 1D bottom relief $H(x)$.

$f_m^\varepsilon(x,y,t)$ from underwater systems (DART buoys, tide gauges measurements) at ε-neighborhoods of points $(x_m, y_m) \in \Omega$

$$\eta(x,y,t) = f_m^\varepsilon(x,y,t), \qquad x \in (x_m - \varepsilon, x_m + \varepsilon),\ y \in (y_m - \varepsilon, y_m + \varepsilon),\ \varepsilon > 0, \\ t \in (T_m^{(1)}, T_m^{(2)}),\ m = 1, 2, \ldots, M. \tag{2}$$

Inverse problem 2 (IP 2): find $q(x,y)$ from (1) using function $H(x,y)$ and satellite altimeters data $F_2(x,y)$

$$\eta(x,y,T) = F_2(x,y), \quad (x,y) \in \omega \subset \Omega,\ T > 0. \tag{3}$$

Here $\omega := (l_x^{(1)}, l_x^{(2)}) \times (l_y^{(1)}, l_y^{(2)})$ is a subset of Ω.

Inverse problem 3 (combined IP 3): find $q(x,y)$ from (1)-(3) using function $H(x,y)$, measured data $f_m^\varepsilon(x,y,t)$, $m = 1, \ldots, M$, and $F_2(x,y)$.

Let us present inverse problems 1, 2 and 3 in the operator form: $A_i q = F_i$, $i = 1,2,3$. Here $A_1 : \mathbf{H}^2(\Omega) \mapsto C(\Omega_T; E^M)$, $A_2 : \mathbf{H}^2(\Omega) \mapsto L_2(\Omega)$ and $A_3 := (A_1, A_2)^T$, $F_1 := (f_1^\varepsilon, f_2^\varepsilon, \ldots, f_M^\varepsilon) \in E^M$ is the vector of discrete output data depends on (x,y,t), $F_3 = (F_1, F_2)^T$, E^M is Euclidean space. The inverse problem 3 is ill-posed because A_3 is a compact operator [1]. The compactness of operators A_1 and A_2 is established in papers [2] and [11, 12, 9], respectively. We will find the solution $q(x,y)$ of inverse problems in the class of functions $q(x,y) = \sum\limits_{k=1}^{K} q_k(x) \sin(2\pi k y / L_y)$ which means that we regularize our inverse problems using cut Fourier series [1].

3 VARIATIONAL FORMULATION OF INVERSE PROBLEMS

Inverse problems $A_i q = F_i$ can be reduced to the minimization problems $\min\limits_{q \in H^2(\Omega)} J_i(q)$, $i = 1,2$ [1]. Here $J_i(q) = \|A_i q - F_i\|^2$ are cost functions, $i = 1,2$.

In this section we find gradients of cost functions $J_i(q)$, $i = 1,2$, and introduce a cost function $J_3^{(\beta)}(q)$ for the combined IP 3.

3.1 Inverse problem 1

The conditions of well-posedness of IP 1 in one-dimensional case are given in [13]. The algorithm of constructing function $q(x, y)$ in two-dimensional case based on truncated singular value decomposition is proposed in [6, 7, 14].

The cost function $J_1(q)$ for IP 1 has the form:

$$J_1(q) = \|A_1 q - F_1\|^2_{L^2(0,T)} := \sum_{m=1}^{M} \int\limits_{T_m^{(1)}}^{T_m^{(1)}} \int\limits_{x_m-\varepsilon}^{x_m+\varepsilon} \int\limits_{y_m-\varepsilon}^{y_m+\varepsilon} [\eta(x, y, t; q) - f_m^{\varepsilon}(x, y, t)]^2 \, dy \, dx \, dt.$$

Lemma 1 [2]. *The gradient of the cost function $J_1(q)$ has the form $J_1' q = \psi_{1_t}(x, y, 0)$. Here $\psi_1 \in C(\Omega_T; \mathbf{H}^2(\Omega))$ is the weak solution of the following problem:*

$$\begin{cases} \mathcal{L}\psi_1 = R_1(x, y, t), & (x, y) \in \Omega,\ t \in (0, T), \\ \psi_1(x, y, T) = 0,\ \psi_{1_t}(x, y, T) = 0, & (x, y) \in \Omega, \\ \psi_1|_{\partial\Omega_T} = 0, & t \in (0, T), \end{cases} \tag{4}$$

$R_1(x, y, t) = -2 \sum\limits_{m=1}^{M} \{[\eta(x, y, t) - f_m^{\varepsilon}(x, y, t)]\theta(x - x_m + \varepsilon)\theta(x_m + \varepsilon - x) \cdot \theta(y - y_m + \varepsilon)\theta(y_m + \varepsilon - y)\theta(t - T_m^{(2)})\theta(T_m^{(2)} - t)\}.$

3.2 Inverse problem 2

The cost function $J_2(q)$ for IP 2 has the form:

$$J_2(q) = \|A_2 q - F_2\|^2_{L^2(0,T)} := \int\limits_{l_x^{(1)}}^{l_x^{(2)}} \int\limits_{l_y^{(1)}}^{l_y^{(2)}} (\eta(x, y, T) - F_2(x, y))^2 \, dy \, dx.$$

Lemma 2 [8, 15]. *The gradient of the cost function $J_2(q)$ has the form $J_2' q = \psi_{2_t}(x, y, 0)$. Here $\psi_2 \in \mathbf{H}^2(\Omega)$ is the weak solution of the following problem:*

$$\begin{cases} \mathcal{L}\psi_2 = 0, & (x, y) \in \Omega, t \in (0, T); \\ \psi_2(x, y, T) = 0,\ \psi_{2_t}(x, y, T) = R_2(x, y), & (x, y) \in \Omega; \\ \psi_2|_{\partial\Omega_T} = 0, & t \in (0, T) \end{cases}$$

$R_2(x, y) = 2\,(\eta(x, y, T) - F_2(x, y))\,\theta(x - l_x^{(1)})\theta(l_x^{(2)} - x) \cdot \theta(y - l_y^{(1)})\theta(l_y^{(2)} - y).$

3.3 Inverse problem 3

We introduce the cost function $J_3^{(\beta)}(q)$ for IP 3 in the form: $J_3^{(\beta)}(q) = \beta J_1(q) + (1 - \beta)J_2(q)$, $\beta \in [0, 1]$. The gradient of a cost function $J_3^{(\beta)}(q)$ has the form: $J_3^{(\beta)\prime} q = \beta J_1' q + (1 - \beta)J_2' q$.

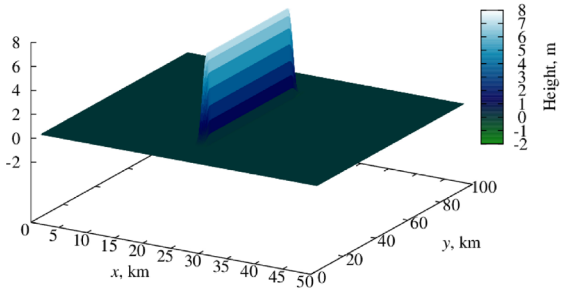

Figure 3: The exact solution $q_e(x, y)$ of inverse problems.

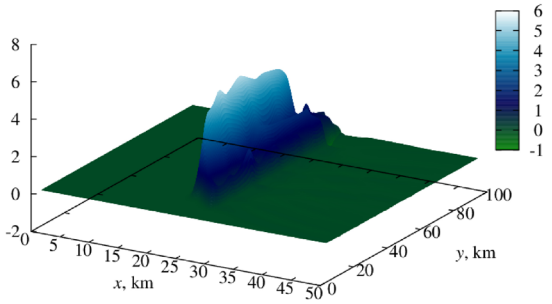

Figure 4: The reconstructed solution $q_5^{(1)}(x, y)$ of IP 1 from the random noisy output data with $\gamma = 3\%$.

4 RESULTS OF NUMERICAL CALCULATION

We apply the conjugate gradient method [16, 1] for solving IP 1, IP 2 and IP 3 numerically.

We choose the following parameters for numerical experiments: $L_x = 50$ km, $L_y = 100$ km, $T = 60$ min, $\varepsilon = 125$ m, $N_x = 750$, $N_y = 500$, $N_t = 600$. The bottom is assumed to be one-dimensional (see figure 2) with the highest $H_{\max} = 6$ km and lowest $H_{\min} = 5$ m average depth of the ocean. We choose an exact solution $q_e(x, y)$ of inverse problems with a wave height $A = 8$ m (see figure 3). We use the explicit finite-difference conservative scheme of the second order approximation [2] with Courant condition $h_t = 0,8 \cdot h_x h_y \left(h_x^2 + h_y^2\right)^{-1/2} / \|c\|_C$. We set data f_m^ε, $m = \overline{1,6}$, and F_2 with "white" noise 1-7%, *i.e.* $f_m^{\varepsilon,\gamma}(x, y, t) = f_m^\varepsilon(x, y, t) + \gamma \text{Random}(f_m^\varepsilon)\|f_m^\varepsilon\|$, $\gamma \in (0.01, 0.07)$. Noise data for IP 1 is generated from the discrete numerical solution of the direct problem in six points (x_m, y_m) equally-spaced on the interval $((40, 15); (47, 89))$. We choose an initial approximation $q_0 = H_{\max}$ which corresponds to an unperturbed sea surface.

We use the stopping condition $J_i(q_n) < \varepsilon_s$, $i = 1, 2$, where choosing of $\varepsilon_s > 0$ based on analysis of deficiency [2]. The behaviour of deficiency as a function of the iteration number n consists of three phases: the initial phase of rapid decrease but short duration, the second phase of slow decrease, and the third phase of almost constant behavior, after some iterations. The numerical results show the minimum value of difference between exact q_e and approximate q_n solutions is achieved between the second and third phases of the deficiency curve versus n.

Let us denote $q_n^{(i)}$, $i = 1, 2$, is n-th approximation of the solution of IP 1 and 2. The reconstructed solution $q_n^{(1)}$ of IP 1 from the random noisy output data $\gamma = 3\%$ is demonstrated on figure 4.

For solving numerically IP 2 we put $\omega = (0, 25) \times (0, 50)$ km. The reconstructed solution $q_n^{(2)}$ of IP 2 from the random noisy output data $\gamma = 3\%$ is demonstrated on figure 5.

The reconstructed solution $q_{n,\beta}^{(3)}$ of IP 3 from the random noisy output data with $\gamma = 3\%$, $\beta = 0.3$, is demonstrated on figure 6. Note, that the location of initial source as well as

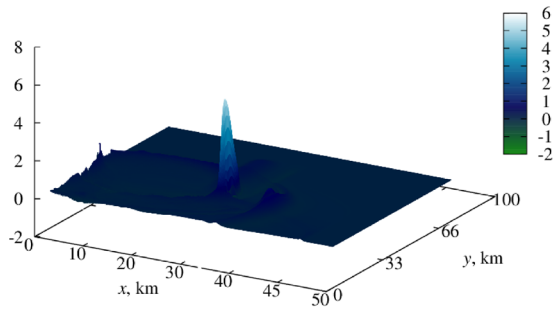

Figure 5: The reconstructed solution $q_{15}^{(2)}(x,y)$ of IP 2 from the random noisy output data with $\gamma = 3\%$.

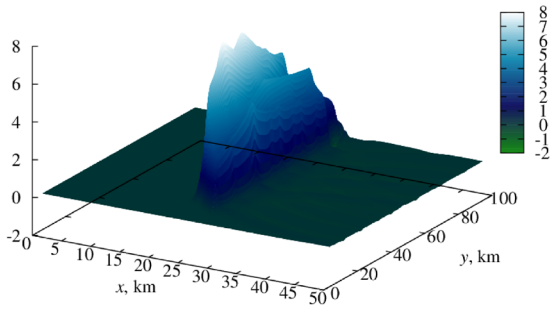

Figure 6: The reconstructed solution $q_{4,\beta}^{(3)}(x,y)$ of IP 3 from the random noisy output data with $\gamma = 3\%$.

its amplitude is reconstructed better than in case of IP 1 and IP 2. The parameter β in combined function $J_3^{(\beta)}(q)$ depends on sensitivity of the functional $J_1(q)$ and $J_2(q)$ (figure 7).

We compare relative accuracy error curves $E_i(n; q^{(i)}; \gamma) = \|q_e - q_n^{(i)}\|/\|q_e\|$, $i = 1, 2$, for IP 1, 2 and $E_3(n; q_\beta^{(3)}; \gamma)$ for IP 3. Figure 7 shows that using of combined underwater systems and satellite data allows one to increase the stability and efficiency of tsunami source reconstruction.

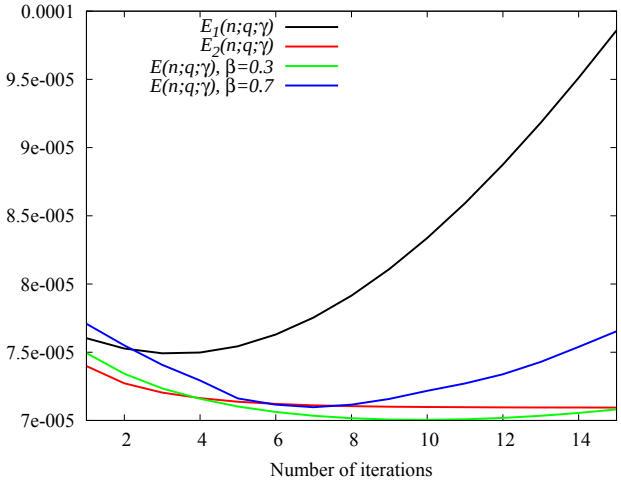

Figure 7: The relative accuracy errors $E_i(n; q^{(i)}; \gamma)$, $i = 1, 2, 3$, for IP 1, IP 2 and IP 3 for $\beta = 0.3$ and $\beta = 0.7$. Note, that curves E_3 are located below curves E_i, $i = 1, 2$, for $n = 7$ when $\beta = 0.7$ (blue line) and $n = 5, 6, \ldots, 14$ when $\beta = 0.3$ (green line).

Note, that after reconstruction $q(x, y)$ we can calculate the amplitude of the tsunami wave using Airy-Green formula in case of 1D bottom profile (figure 2) [17]. In case of 2D bottom profile and linear source $q(x, y) = g(y)\delta(x)$ we can solve 2D direct problem for the amplitude $S(z, y)$

$$\begin{cases} S_z + 0.5a_1 S_y + 0.5a_2 S = 0, & z > 0, y \in (-\infty, +\infty); \\ S(0, y) = g(y), & y \in (-\infty, +\infty) \end{cases}$$

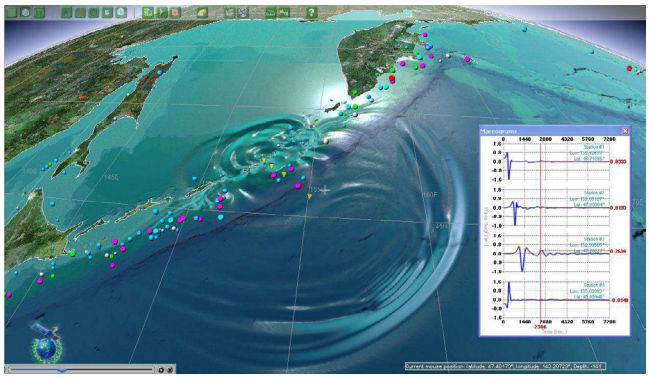

Figure 8: Numerical modelling of the Simushir tsunami 13.01.2007 using the built-in software.

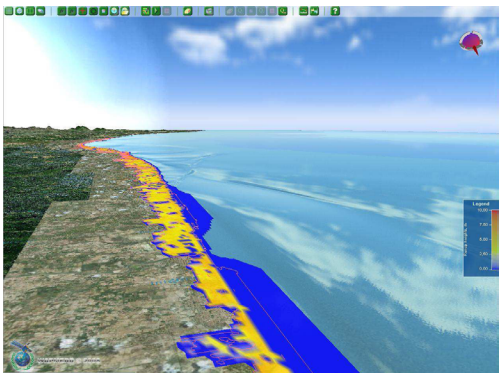

Figure 9: The flooding map of Nagapattinam, India, after tsunami run-up.

which coincides with Airy-Green formula in 1D case: $S(x) = \sqrt[4]{H(0)/H(x)}$. Here new variable $z = \tau(x, y)$ denotes the solution of eikonal equation $\tau_x^2 + \tau_y^2 = (gH(x, y))^{-1}$, a_1 and a_2 depend on $H(x, y)$ [17].

5 3D VISUALIZATION SYSTEM

Non-profit organization WAPMERR (World Agency of Planetary Monitoring and Earthquake Risk Reduction) in collaboration with GeoSystema Ltd. and ICM&MG SB RAS developed the Integrated Tsunami Research and Information System (ITRIS) to simulate tsunami waves and earthquakes, river course changes, coastal zone floods, and risk estimates for coastal constructions at wave run-ups and earthquakes [18]. The special scientific plug-in components are embedded in a specially developed GIS-type graphic shell for easy data retrieval, visualization and processing (see figure 8). A series of preliminary numerical experiments on the simplified three-dimensional models with invariable forcing is conducted based on the computational technology. These experiments give particular examples of fluid dynamics while interacting with external objects. The presented software can be used for analysis and research of various natural and man-made hazards. Figure 9 demonstrates the flooding map of artificial tsunami run-up near the Nagapattinam, India. For run-up modelling we solve nonlinear shallow water equations by the finite volume method. The main advantages of this method are using Total Variation Diminishing for stability control, high speed of calculations and adaptation for any topography of settlement area.

There are built-in catalogues and databases with set of interfaces for data managing. Fig. 10 present visualization of earthquake epicentres and tsunami locations around Japan.

The ICM&MG SB RAS develops mathematical and computational methods for Arctic region. The coupled model consisting of blocks for blocks of model of dynamics of the ocean, model of dynamics of the atmosphere and their interaction block is adapted for the computing platform of the supercomputer. A new method of observational data

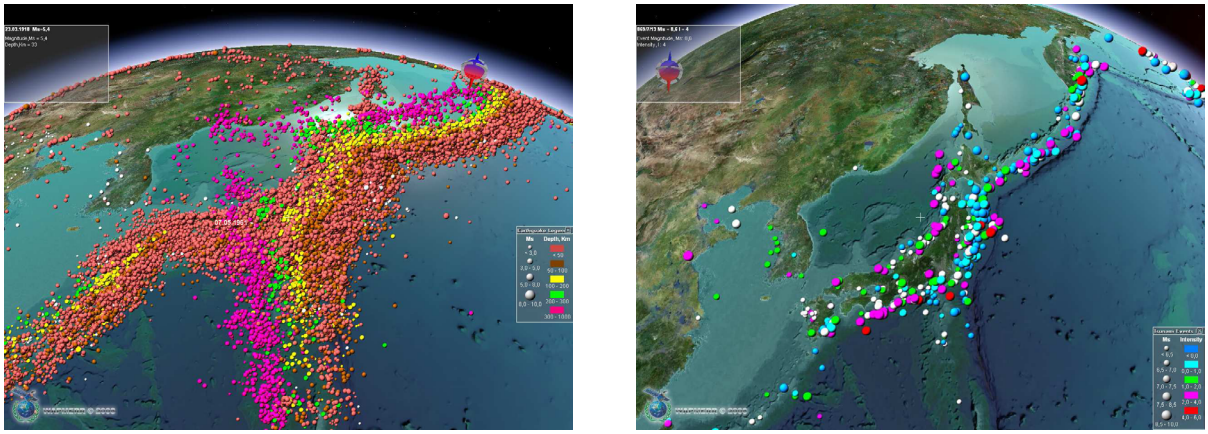

Figure 10: Visualization of the available seismic data (left) and tsunami locations (right) around Japan.

assimilation is elaborated, which is based on properties of diffusive random processes. Data on the Arctic region for the subsequent assimilation in the model are collected and programs for selection and control of these data are created.

ACKNOWLEDGMENTS

This work is supported by the Ministry of Education and Science of the Russian Federation and by the Russian Foundation for Basic Research (project No. 15-01-09230).

REFERENCES

[1] Kabanikhin, S.I. *Inverse and Ill-Posed Problems: Theory and Applications*. Berlin: de Gruyter, 2011.

[2] Kabanikhin, S., Hasanov, A., Marinin, I., Krivorotko, O. and Khidasheli, D. A variational approach to reconstruction of an initial tsunami source perturbation. *Appl. Numer. Math.* (2014) **83**:22-37.

[3] Vreugdenhil, C. V. *Numerical Methods for Shallow-Water Flow*. The Netherlands: Springer, 1994.

[4] Pelinovsky, E. *Waves in Geophysical Fluids. Tsunamis, Rogue Waves, Internal Waves and Internal Tides*, ed. J Grue and K Trulsen, Norway: SpringerWien-NewYork, 2006.

[5] Dutykh, D., Mitsotakis, D., Chubarov, L.B. and Shokin, Y.I. On the contribution of the horisontal sea-bed displacements into the tsunami generation process. *Ocean Modelling*. (2012) **56**:43-56.

[6] Voronina, T.A. and Tcheverda, V.A. Reconstruction of tsunami initial form via level oscillation. *Bull. Novosib. Comput. Cent., Ser. Math. Model. Geophys.* (1998) **4**:127-136.

[7] Voronina, T.A. Reconstruction of initial tsunami waveforms by a truncated SVD method. *J. Inverse Ill-Posed Probl.* (2011) **19**:615-629.

[8] Kabanikhin, S.I., Bektemesov, M.A., Nurseitov, D.B., Krivorotko, O.I. and Alimova, A.N. An optimization method in the Dirichlet problem for the wave equation. *J. Inverse Ill-Posed Probl.* (2012) **20**:193-211.

[9] Kabanikhin, S.I. and Krivorotko, O.I. Combined inverse tsunami problem. *Bull. Novosib. Comput. Cent., Ser. Math. Model. Geophys.* (2013) **16**:45-58.

[10] Kabanikhin, S. and Krivorotko, O. Optimization approach to combined inverse tsunami problem. *Proc. Inverse Problems – from Theory to Applications, Bristol, UK, 26-28 August, 2014*:102-107.

[11] Ivanov, V.K., Vasin, V.V. and Tanana, V.P. *Theory of Linear Ill-posed Problems and its Applications*. Boston: VSP, Vol. 36, 2002.

[12] Anikonov, Yu.E., Bubnov, B.A. and Erokhin, G.N. *Inverse and Ill-posed Sources Problems*. The Netherlands: VSP, Vol. 9, 1997.

[13] Romanov, V.G. and Moshkalev, P.S. The one-dimensional inverse problem of finding a tsunami source. *Journal of Applied and Industrial Mathematics* (2011) **14**:87-99.

[14] Voronina, T.A. and Voronin, V.V. Properties of the inverse problem operator for reconstructing the tsunami source. *Bull. Novosib. Comput. Cent., Ser. Math. Model. Geophys.* (2014) **17**:73-84.

[15] Kabanikhin, S.I. and Krivorotko, O.I. The numerical method of solving Dirichlet problem for the wave equation. *Journal of Applied and Industrial Mathematics* (2012) **15**:90-101.

[16] Hanke, M. *Conjugate Gradient Type Methods for Ill-Posed Problems*. England: Longman Scientific & Technical, 1995.

[17] Kabanikhin, S.I. and Krivorotko, O.I. A numerical method for determining the amplitude of a wave edge in shallow water approximation. *Appl. Comput. Math.* (2013) **12**:91-96.

[18] Kabanikhin, S.I., Krivorotko, O.I. and Marinin, I.V. *3D GIS for Research of Natural and Technogenic Emergency Situations*. Moscow: Palmarium Academic Publishing, 2013.